

Impact of Canopy Representations on Regional Modeling of Evapotranspiration using the WRF-ACASA Coupled Model

Liyi Xu, Rex Dave Pyles, Kyaw Tha Paw U, Richard Snyder,
Erwan Monier, Matthias Falk and Shu-Hua Chen



Report No. 287
December 2015

The MIT Joint Program on the Science and Policy of Global Change combines cutting-edge scientific research with independent policy analysis to provide a solid foundation for the public and private decisions needed to mitigate and adapt to unavoidable global environmental changes. Being data-driven, the Program uses extensive Earth system and economic data and models to produce quantitative analysis and predictions of the risks of climate change and the challenges of limiting human influence on the environment—essential knowledge for the international dialogue toward a global response to climate change.

To this end, the Program brings together an interdisciplinary group from two established MIT research centers: the Center for Global Change Science (CGCS) and the Center for Energy and Environmental Policy Research (CEEPR). These two centers—along with collaborators from the Marine Biology Laboratory (MBL) at Woods Hole and short- and long-term visitors—provide the united vision needed to solve global challenges.

At the heart of much of the Program's work lies MIT's Integrated Global System Model. Through this integrated model, the Program seeks to: discover new interactions among natural and human climate system components; objectively assess uncertainty in economic and climate projections; critically and quantitatively analyze environmental management and policy proposals; understand complex connections among the many forces that will shape our future; and improve methods to model, monitor and verify greenhouse gas emissions and climatic impacts.

This reprint is one of a series intended to communicate research results and improve public understanding of global environment and energy challenges, thereby contributing to informed debate about climate change and the economic and social implications of policy alternatives.

Ronald G. Prinn and John M. Reilly,
Program Co-Directors

For more information, contact the Program office:

MIT Joint Program on the Science and Policy of Global Change

Postal Address:

Massachusetts Institute of Technology
77 Massachusetts Avenue, E19-411
Cambridge, MA 02139 (USA)

Location:

Building E19, Room 411
400 Main Street, Cambridge

Access:

Tel: (617) 253-7492

Fax: (617) 253-9845

Email: globalchange@mit.edu

Website: <http://globalchange.mit.edu/>

Impact of Canopy Representations on Regional Modeling of Evapotranspiration using the WRF-ACASA Coupled Model

Liyi Xu^{*†}, Rex Dave Pyles[‡], Kyaw Tha Paw U[‡], Richard Snyder[‡], Erwan Monier^{*}, Matthias Falk[‡] and Shu-Hua Chen[‡]

Abstract

In this study, we couple the Weather Research and Forecasting Model (WRF) with the Advanced Canopy-Atmosphere-Soil Algorithm (ACASA), a high complexity land surface model, to investigate the impact of canopy representation on regional evapotranspiration. The WRF-ACASA model uses a multilayer structure to represent the canopy, consequently allowing microenvironmental variables such as leaf area index (LAI), air and canopy temperature, wind speed and humidity to vary both horizontally and vertically. The improvement in canopy representation and canopy-atmosphere interaction allow for more realistic simulation of evapotranspiration on both regional and local scales. Accurate estimates of evapotranspiration (both potential and actual) are especially important for regions with limited water availability and high water demand, such as California. Water availability has been and will continue to be the most important issue facing California for years and perhaps decades to come. Terrestrial evapotranspiration is influenced by many processes and interactions in the atmosphere and the bio-sphere such as water, carbon, and momentum exchanges. The need to improve representation within of surface-atmosphere interactions remains an urgent priority within the modeling community.

Contents

1. INTRODUCTION	1
2. MODELS, METHODOLOGY AND DATA	3
2.1 Models	3
2.2 Data	5
2.3 Model Setup	6
3. RESULTS AND DISCUSSION	8
3.1 Reference Evapotranspiration	8
3.2 Actual Evapotranspiration	15
4. SUMMARY AND CONCLUSION	20
5. REFERENCES	21

1. INTRODUCTION

The land surface is an important component that contributes to the evolution of atmospheric processes. Complex interactions between the atmosphere and land surface drive the impacts of energy, momentum, heat, water, and gas exchanges on atmospheric motions. Many of these effects are attributed to the presence of vegetation in the surface layer (Potter *et al.*, 1993; Dickinson and Henderson-Sellers, 2006; Dirmeyer *et al.*, 2010), which is a crucial part of the land surface layer, representing 99% of the mass of surface biota. Because of this, land surface parameterization in atmospheric models must emphasize the processes associated with vegetation.

^{*}Joint Program on the Science and Policy of Global Change, Massachusetts Institute of Technology, Cambridge, MA, USA.

[†]Corresponding author (Email: liyixm@mit.edu)

[‡]Department of Land, Air, and Water Resources, University of California Davis, Davis, California, USA

Effects of climate on vegetation phenology have long been a research focus in the ecology and plant science communities (Levitt *et al.*, 1980; Jones, 1992). Climate conditions such as temperature, humidity, and radiation strongly influence plant physiological responses in photosynthesis, respiration, transpiration, and energy flux. However, the influences of vegetation on the climate and atmospheric processes are not as well understood due to numerical complexity and related challenges that arise from properly representing exchanges between the physiologically active vegetated land surfaces and the atmosphere. In recent years, research interests in land and atmospheric interactions have grown considerably, benefitting from the developments of atmosphere and land surface models as well as advanced instrumentation and field campaigns.

Land cover type and vegetation amount are related factors that characterize biosphere-atmosphere interactions. Differences in land use cover can dramatically influence land surface processes by altering surface roughness, canopy transmission of light, physiological responses to environmental controls, and interception of precipitation. Vegetation amount is quantified with the leaf area index (LAI), which is a representation of the total leaf area over a given area of land. Leaves provide surface area for photosynthesis, respiration, and transpiration that control the moisture and energy exchanges with the atmosphere. Specifically, the LAI strongly influences the amount of absorbed solar radiation and its partitioning into sensible and latent energy fluxes. Studies using General Circulation Models (GCMs) have demonstrated the importance and influence of LAI on the short- and long-term evolution of surface hydrology, including snowpack evolution, soil wetness, and evapotranspiration (ET) (Chase *et al.*, 1996; Pitman *et al.*, 1999; Bounoua *et al.*, 2000; Hales *et al.*, 2004). Gao *et al.* (2008) further examined the sensitivities of land surface climate to the changes in spatial distribution of LAI from different treatments of surface properties: natural inter-annually varying vegetation versus a 10-year climatological annual cycle. Overall, the study showed that observed inter-annually varying vegetation properties led to improvement in estimations of surface fluxes such as latent heat and surface evapotranspiration, regional surface temperature, and spatial distribution of precipitation.

Actual evapotranspiration (ET_a) is the water loss rate by transpiration from plants and evaporation from both soil and vegetation. The standardized Reference evapotranspiration (ET_o) is the evaporative loss rate from a virtual 0.12 m tall vegetated surface having known canopy and aerodynamic resistance (Allen *et al.*, 2005). Although ET_o is technically defined for a virtual surface, it provides a good estimate of the evapotranspiration from a surface covered by 0.12 m tall cool-season grass with adequate water supply. Vegetation representations of most plants are by definition not directly included in the ET_o; however, the response of ET_o to environmental variables is closely linked to the response of actual evapotranspiration. The accurate estimations of ET_o and ET_a are crucial for optimal water management practices and drought monitoring, especially for regions with limited water availability and high water demand, such as the Central Valley of California.

Reference evapotranspiration (ET_o) provides a type of environmentally controlled physiological standard model that is useful in assessing potential environmental controls on ET_a. In reality, the land surface is covered by diverse vegetation ranging such as grasslands, mixed woodlands, and forests; their existence at any location is a result of the complex interaction of anthropogenic

activity, ecological constraints, and environmental controls including water availability. Hence, the ET_a commonly differs from the ET_o , mainly due to differences in the transpiration component of ET. The ET_a rate ranges from zero up to a potential evapotranspiration (ET_c), which is limited by energy availability for vaporizing water. When soil water content is adequate, $ET_a=ET_c$, and ET_a decreases relative to ET_c when soil water (rather than energy availability) limits evapotranspiration.

Transpiration from vegetated surfaces accounts for significant amounts of water entering the atmosphere. 70% of the total precipitation on the continental United States and 85% of total evapotranspiration from the Amazon rainforest are cycled at least once through leaf transpiration (Shuttleworth, 1984). In addition to environmental conditions, the canopy vegetation also controls the overall transpiration rate physiologically and physically, by opening and closing stomata to regulate energy and gas exchanges and by the sheer amount of leaf area available for this activity in response to light and water stress. Many processes and interactions in the atmosphere and biosphere influence plant and soil water losses by evapotranspiration. The need to improve representation within surface-atmosphere interactions remains an urgent priority within the modeling community.

Motivated by Gao *et al.* (2008) and previous studies, this research extended the earlier works involving coarse resolution GCMs to examine the impacts of land surface representations in regional models (Abramowitz *et al.*, 2008; Henderson-Sellers *et al.*, 1996; Chen *et al.*, 1997). Here, to simulate evapotranspiration over California's diverse terrain and ecosystems, the mesoscale Weather Research and Forecasting model (WRF) is used with two land surface models (LSMs) having two distinct levels of complexity: the intermediate complexity NOAH and the complex Advanced Canopy-Atmosphere-Soil Algorithm (ACASA).

The objective of this paper is to investigate how the variability of Reference (ET_o) and Actual (ET_a) evapotranspiration is influenced by the surface representation, such as leaf area index, and the land surface model complexity. Both reference and actual evapotranspiration are important to an understanding of the hydrologic cycle, vegetation dynamics, and surface energy balances in the surface layer. They are also important variables for use in water management, drought monitoring, agricultural production, and fire hazard management. The effects of leaf area index and model complexity on reference evapotranspiration—which is completely dependent on atmospheric conditions—represents the vegetated controls on the atmosphere that can feedback to the land surface. The simulated actual evapotranspiration includes the feedback processes and represents the complete interaction between the atmosphere and the vegetation.

2. MODELS, METHODOLOGY AND DATA

2.1 Models

In this study, the Advanced Research WRF (ARW) model Version 3.1 is used to perform climate simulations over California. WRF is a state-of-the-art, mesoscale numerical weather prediction and atmospheric research model developed by a collaborative effort of the National Center for Atmospheric Research (NCAR), the National Oceanic and Atmospheric Administration (NOAA), the Earth System Research Laboratory (ESRL), and many other agencies. The WRF

model contains a nearly complete set of compressible and non-hydrostatic equations for atmospheric physics (Chen and Dudhia, 2000). The high spatial and temporal resolution of the WRF model is essential for simulating climate over the intricate terrains and land covers of California. The physical parameterizations used in this study are described in more detail in Xu *et al.* (2014).

The land surface models used in this study are the NOAH model (Mahrt and Ek, 1984; Chen and Dudhia, 2000) and the ACASA model (Meyers, 1985; Meyers and Paw U, 1987; Pyles, 2000; Pyles *et al.*, 2000). The two models differ significantly in the complexity of the representation of plant physiology and biometeorological processes. While NOAH is widely used for both climate studies and weather forecasting, it is an intermediate complexity model with multiple soil layers but only a single canopy layer. It scales the single leaf-based physical and physiological processes to represent the whole canopy using bulk similarity assumptions. The ACASA model is a higher-complexity model that includes many plant physiological and biometeorological processes (i.e., photosynthesis and respiration) that are not represented in the NOAH model. It uses multi-layer canopy structures and multiple sun angles within each layer to represent the canopy. These subsequently allow variables such as LAI, air and canopy temperature, wind speed and humidity to also vary vertically. The surface layer is divided into 10 canopy layers and 10 above-canopy layers. Within each canopy layer there are 10 leaf angle classes—9 sunlit angle at 10-degree intervals and 1 shaded—to represent differential illumination of canopy surfaces. A third order turbulent closure scheme used in the ACASA model allows both down- and counter-gradient transport, which are not presented in the NOAH model.

Of particular importance is the role of Leaf Area Index (LAI) in controlling the surface processes in the two land surface models. LAI in the NOAH model is primarily used to calculate the bulk canopy resistance of the single surface layer. Canopy resistance for vegetation transpiration and energy partitioning is estimated using the Jarvis parameterization, where canopy resistance R_c is a function of $R_{c,min}$ (a single prescribed minimum canopy resistance specified by plant functional type), LAI, and F_1 , F_2 , F_3 , and F_4 , which account for the effects of radiation, temperature, humidity, and soil moisture (Jacquemin and Noilhan, 1990; Chen and Dudhia, 2001a,b).

$$R_c = \frac{R_{c,min}}{LAI(F_1 F_2 F_3 F_4)} \quad (1)$$

In the ACASA model, LAI is used to create vertical profiles for multilayer canopy structures. Depending on land-use cover, the LAI values affect light and precipitation interception and alter the canopy energy budgets. The model calculates canopy resistance and stomatal resistance at the leaf surface of each vertical layer using a combination of the Ball- Berry stomatal conductance (Leuning, 1990; Collatz *et al.*, 1991) and the Farquhar *et al.* (1982) photosynthesis equation used in Su *et al.* (1996).

$$g_{s,w} = m \frac{A_n}{c_s} r h_s + b \quad (2)$$

$$rh_s = \frac{g_b q_A + g_{s,w} q_s(T_L)}{g_b + g_{s,w} q_s(T_L)} \quad (3)$$

$$c_s = c_A - \frac{A_n}{g_b} \quad (4)$$

where $g_{s,w}$ is the leaf stomatal conductance to water vapor, A_n is the net CO₂ uptake rate at the leaf surface, c_s and rh_s are the CO₂ concentration and the fractional relative humidity at the leaf surface, m and b are empirical regression coefficients; c_A is the CO₂ concentration in air, $q_s(T_L)$ is saturated mixing ratio of water vapor at leaf temperature T_L , g_b is the leaf boundary layer conductance, and q_A is the mixing ratio of water vapor in the air. Because evapotranspiration is an inevitable result of plant physiological processes, oversimplifying the linkage between moisture and carbon dioxide fluxes in land surface processes can lead to the loss of vital information that impact climate simulations (Zhan and Kustas, 2001; Houborg and Soegaard, 2004).

2.2 Data

In this study, WRF simulations are forced by the Northern America Regional Reanalysis (NARR) dataset, which provides input data such as wind speed and direction, temperature, moisture, radiation, and soil temperature to drive the initialization and boundary conditions of the WRF models. The NARR is a regional data set specifically developed for the Northern American region. The temporal and spatial resolutions of this data set are 3-hour intervals and 32-km respectively (Mesinger *et al.*, 2006).

Two leaf area index datasets, USGS and MODIS, are used to drive the surface processes. The default USGS LAI data used by the WRF model prescribes the maximum and minimum LAI values for each point according to plant functional types. Monthly LAI is extrapolated linearly between the maximum and minimum LAI values with monthly Green Vegetation Fraction, which is the fraction of the grid cell covered by active vegetation (Gutman and Ignatov, 1998). The MODIS (Moderate Resolution Imaging Spectroradiometer) dataset is measured daily to provide high spatial and temporal resolution LAI (Knyazikhin *et al.*, 1999). The USGS LAI and MODIS LAI are shown in **Fig. 1** for different seasons of the year 2006. The USGS LAI values are significantly higher than those of the MODIS LAI dataset, especially during the summer months. There is no interannual variability in the WRF USGS LAI, in contrast to the satellite measured MODIS LAI. Both LAI datasets display temporal and spatial differences among the different time of the year over California.

The main independent observational datasets used to evaluate the model simulations were obtained from the California Irrigation Management Information System (CIMIS) for ETo, and the AmeriFlux network for both ETo and ETa (**Fig. 2**). The CIMIS stations are sparsely located, mostly in the Central Valley and Southern Coastal areas. There are only six AmeriFlux sites in California for the study period, even though it is the period with the most active stations, and be-

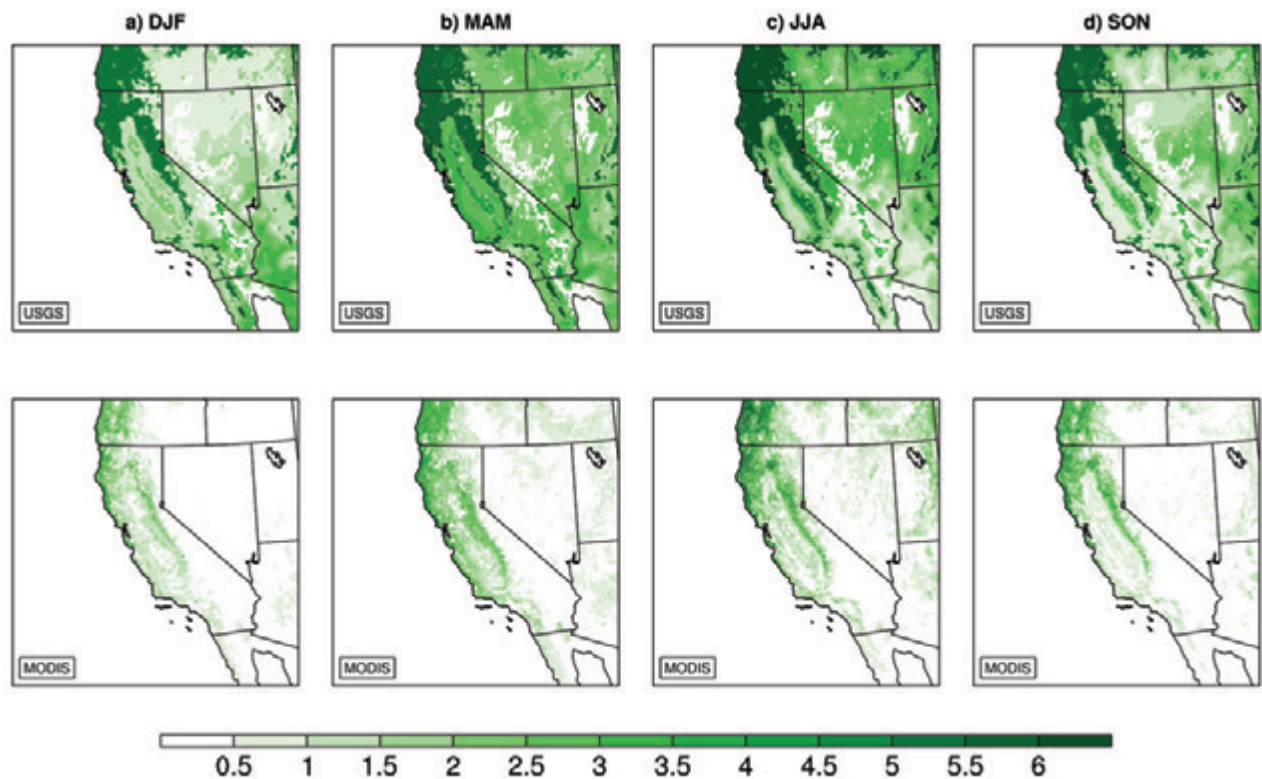


Figure 1. Maps of MODIS LAI and USGS LAI for a) winter: December, January, and February (DJF); b) spring: March, April, and May (MAM); summer: June, July, and August (JJA); and autumn: September, October, and November (SON) of 2006.

cause some stations are very close by each other, only three distinct markers are visible in Fig. 2. Moreover, due to the close proximities of the three Sky Oak sites, they are located within the same WRF model grid cell. Therefore they are not distinguished in the WRF model simulations. The combined coverage of the two datasets still leaves much of California underrepresented for flux observations. Hence, the WRF model can be used as a potentially valuable tool to fill in the temporal and spatial gaps of the surface observations.

In both the ACASA and NOAH models, only the dominant vegetation types or plant functional types (PFTs) are used to represent each grid cell. However, sometime these PFTs do not necessarily represent the observed vegetation type at each of the stations, as shown in **Table 1**. For example, the three Sky Oak sites (USSO2, USSO3, and USSO4) are identified as Evergreen Needleleaf Forest by WRF, instead of the savannas and shrublands that actually surround the sites (observed PFT).

2.3 Model Setup

Four model simulations from the combination of the two land surface models and two LAI representations were used to simulate E_{To} and E_{Ta} across all of California's vast and diverse terrains and ecosystems. The four simulations were: WRF-ACASA with default USGS LAI, WRF-ACASA with high resolution MODIS LAI, WRF-NOAH with USGS LAI, and WRF-NOAH with MODIS LAI. Simulations were performed for the years 2005 and 2006 with horizontal grid

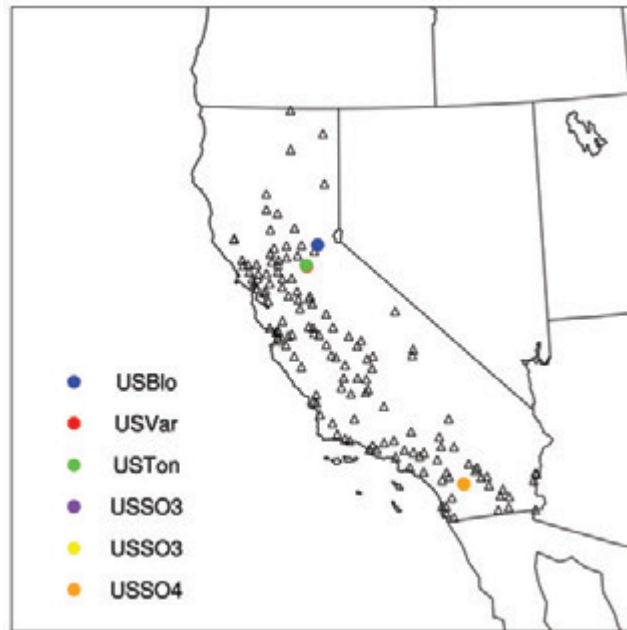


Figure 2. Maps of the 120 CIMIS stations for reference evapotranspiration (ET_o) measurements in triangles, and of the 6 AmeriFlux stations for both reference (ET_o) and actual (ET_a) evapotranspiration measurements in color dots.

spacing of 8 km x 8 km. Besides the differences in the land surface model, all simulations employed the same set of atmospheric physics schemes stemming from the WRF model. These include the Purdue scheme for microphysics (Chen and Sun, 2002), the Rapid Radiative Transfer Model for long wave radiation (Mlawer *et al.*, 1997), the Dudhia scheme for shortwave radiation (Dudhia, 1989), the Monin-Obukhov similarity scheme for surface layer physics of non-vegetated surfaces and the ocean, and the MRF scheme for the planetary boundary layer (Hong and Pan, 1996). WRF runs at a 60-second time step, while the radiation scheme and the land surface schemes are called every 30 minutes. Boundary conditions are specified using NARR. Reference evapotranspiration was calculated using the ET_o equation from Allen *et al.* (2005) with simulated surface air temperature, dew point temperature, solar radiation, and wind speed at 2 m height. Actual evapotranspiration was calculated within the WRF-ACASA and WRF-NOAH models.

For the four simulations, ET_o and ET_a were compared with surface observations to test the hypothesis that terrestrial representations in land surface models influence the simulated evapotranspiration on both local and regional scales. Hourly, daily, monthly and annual temporal scales were used to evaluate the variability of model performance. The comparison between surface observations and model simulations were similar for 2005 and 2006; however, due to the considerable missing observation data during 2005, mainly results from 2006 are presented here.

Some of the challenges in comparing model simulations and the observations are that (1) the measurement heights are sometimes different from the simulated height, and (2) the station landscape could be different from the simulated grid point. Table 1 shows that the measured height varies from site to site for the AmeriFlux network, whereas the models simulate surface temper-

Table 1. Selected sites from the Air Resources Board meteorological stations network.

Station	Site Name	WRF PFT	WRF-ACASA Canopy height (meter)	Observed height (meter)	Observed PFT
NEP	Northeast Plateau	Grassland	1	1.2	Irrigated Grassland
MD	Mojave Desert	Shrubland	3	1.2	Irrigated Grassland
SJV	San Joaquin Valley	Irrigated Cropland and Pasture	1.5	1.2	Irrigated Grassland
MC	Sierra Nevada Mountain	Evergreen Needleleaf Forest	17	1.2	Irrigated Grassland
USBLO	Blodgett Forest	Evergreen Needleleaf Forest	17	12.5	Evergreen Needleleaf Forest
USVAR	Vaira Ranch	Savanna	10	1	Grassland
USTON	Tonzi Ranch	Savanna	10	23	Woody Savannas
USSO2	Sky Oak Old	Evergreen Needleleaf Forest	17	4.2	Woody Savannas
USSO3	Sky Oak Young	Evergreen Needleleaf Forest	17	1	Closed Shrublands
USSO4	Sky Oak New	Evergreen Needleleaf Forest	17	1.5	Closed Shrublands

ature based on a 2 m height. Moreover, this simulated 2 m temperature might be representing the understory of taller plant ecosystems in the WRF-ACASA model (WRF-NOAH does not suffer the same problems; because NOAH is a big-leaf model, the 2-meter height represents a height more similar in characteristics to the observations). In addition, some stations were within patches of specific landscape types that may differ significantly from the assigned overall grid point landscape in WRF. For example, the observed PFT of the three Sky Oak stations from the AmeriFlux data are different from the WRF PFT (Table 1).

3. RESULTS AND DISCUSSION

3.1 Reference Evapotranspiration

The seasonal diurnal patterns of ETo from the four WRF simulations are compared with surface observations from CIMIS stations in **Fig. 3** and the AmeriFlux sites in **Fig. 4**. The seasonal diurnal patterns of the model simulations generally compare well with the surface measurements, and the differences between simulations using USGS LAI and MODIS LAI are small. The Northeast Plateau station and the Blodgett Forest site, where the observed PFTs match the WRF model, show the best model comparisons. However, in the Mojave Desert, San Joaquin Valley and Mountain County stations, where the observed PFTs do not match well with the model plant functional types, both models overestimate the ETo values during daytime of the warmer seasons. The two different LAI datasets do not have a significant impact on the ETo simulations at sub daily scale, though usage of the MODIS LAI slightly improve the WRF-ACASA simulations for the San

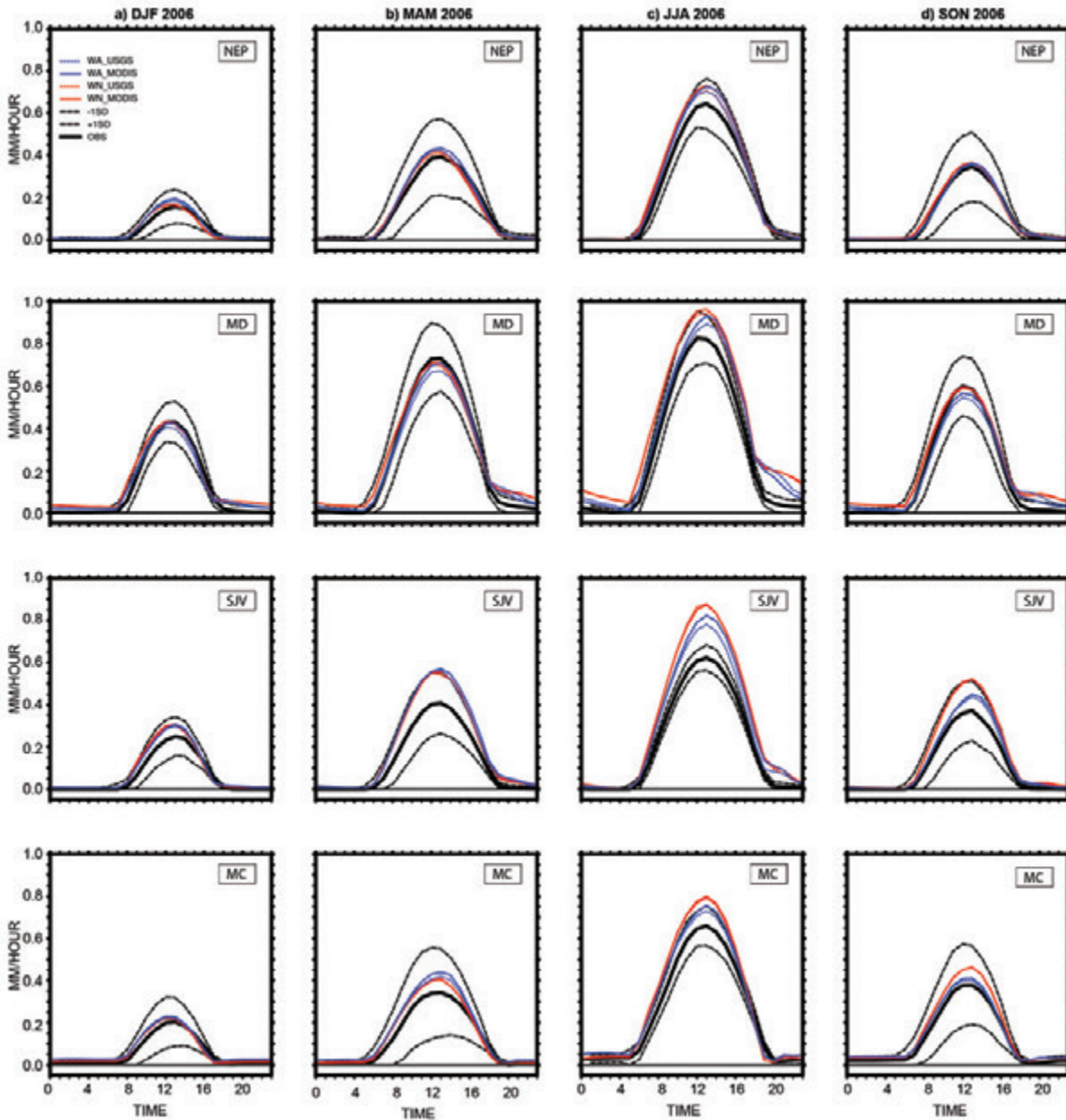


Figure 3. Seasonal diurnal patterns of reference ETo for the four model simulations for the CIMIS stations during 2006. The thick black lines are CIMIS ETo measurements with two dash lines representing one standard deviation above and below the mean diurnal patterns. The red lines are WRF-NOAH simulations and the blue lines are WRF-ACASA simulations. The red and blue dashed lines are for simulations with USGS LAI and the solid lines are for simulations with MODIS LAI. Winter is assumed to be December, January, and February (DJF); spring is March, April, and May (MAM); summer is June, July, and August (JJA); and autumn is September, October, and November (SON).

Joaquin Valley station. Overall, the WRF-ACASA model results exhibit a reduced bias during the daytime.

The time series of the daily ETo from the 2006 CIMIS surface observations as well as the four model simulations are compared in **Fig. 5**. In general, model simulations of daily ETo agree with

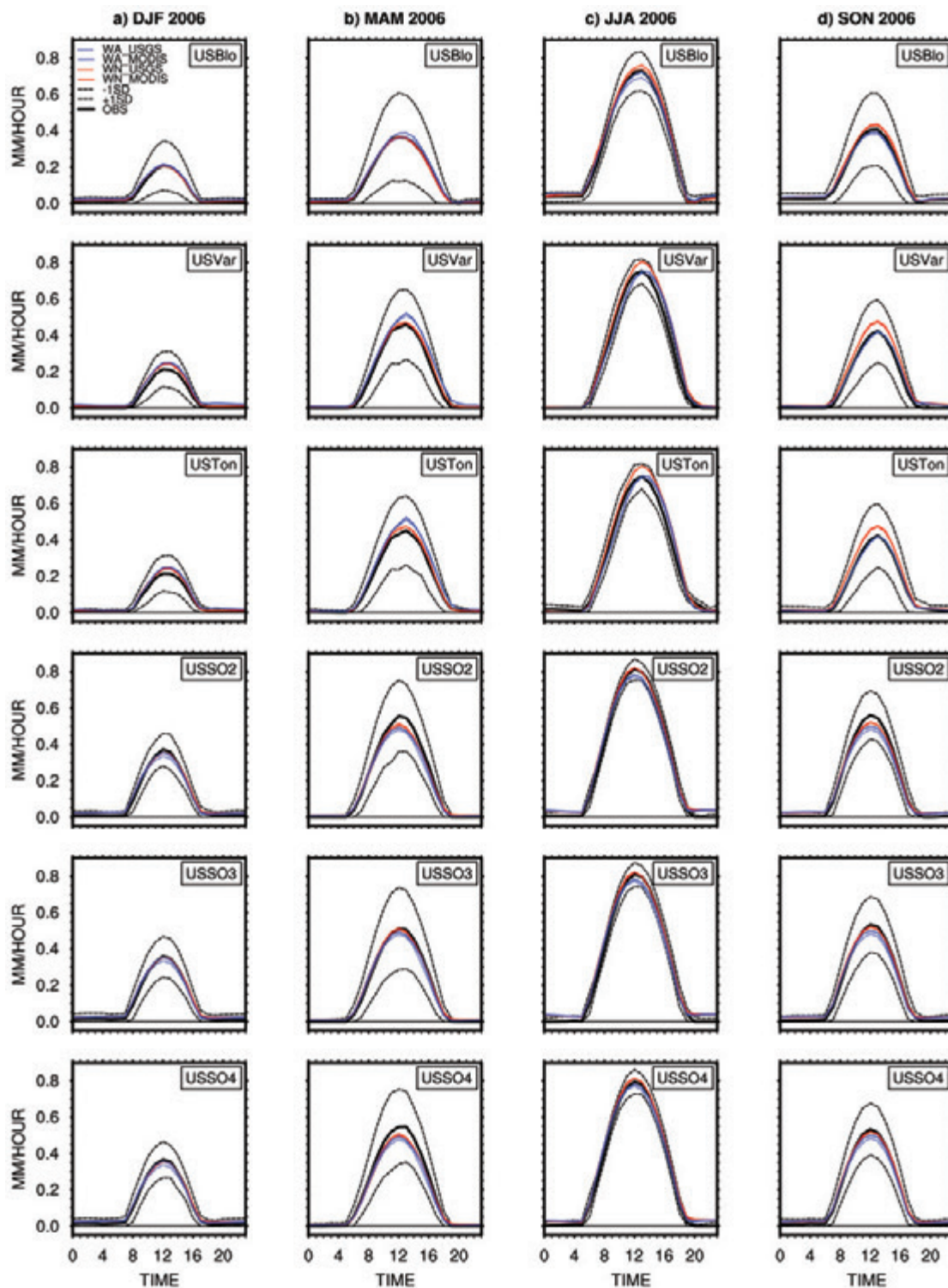


Figure 4. Seasonal diurnal patterns of reference ETo for the AmeriFlux sites during 2006. The thick black lines are observed ETo with two dash lines representing one standard deviation above and below the mean. The red lines are WRF-NOAH simulations and the blue lines are WRF-ACASA simulations. The color dashed lines are for simulations with USGS LAI and the color solid lines are for simulations with MODIS LAI. Winter is (DJF), spring is (MAM), summer is (JJA), and autumn is (SON).

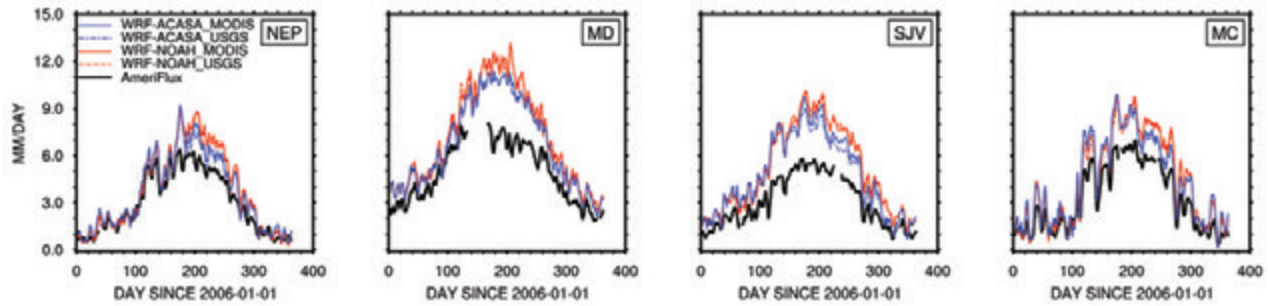


Figure 5. Time series of reference evapotranspiration for the CIMIS stations. The solid black line represents observation. The blue lines are for WRF-ACASA, and the red lines are for WRF-NOAH. The color solid lines are simulations with MODIS LAI, and the color dashed lines are simulations with USGS LAI.

observations during the cool season but depart from the observed trend during the warmer seasons. The overestimation of daily ETo in the time series are results of the daytime bias in ETo (Fig. 3). These small biases, in the order of a few tenths of a millimeter per hour during the daytime, aggregate to be more pronounced in daily values. The sparsely vegetated Mojave Desert and San Joaquin Valley stations are most problematic for the model simulations and experience the most bias overall. **Fig. 6** compares the observed and simulated time series of daily ETo in 2006 for the AmeriFlux sites. In Fig. 6, the timing and magnitude of the simulations agrees well with the surface observations for all sites with small differences over the Varia and Tonzi ranches. This reaffirms the results shown in Fig. 4, which shows simulated diurnal patterns of ETo. The more complex WRF-ACASA model slightly reduces the ETo bias over Vaira and Tonzi Ranch stations in summer and autumn in both hourly and daily scales. This may result from more sophisticated dew point temperature in the WRF-ACASA model where higher complexity in plant physiology representation and multilayer canopy structure improve the moisture exchange within and above the canopy, as shown in Xu *et al.* (2014).

The choice of LAI datasets appears to reveal no significant impact on model results of ETo. Usage of the MODIS LAI slightly increases the daily ETo in the WRF-ACASA model over the WRF-NOAH model. This is a result of lower LAI values in the MODIS dataset increasing the surface air temperature in the WRF-ACASA model and slightly decreasing the relative humidity, thusly increasing the evaporative demand. The annual cumulative reference evapotranspiration over the entire domain for each of the four simulations is shown in **Fig. 7**. Again, LAI does not have a large effect on the annual cumulative ETo when the same model is used. The differences are more results of variation in model complexity. Over the southern Central Valley and southern California, where the San Joaquin Valley and Mojave Desert stations from the CIMIS network are located, the WRF-ACASA simulations have lower annual ETo values than WRF-NOAH. Although both WRF-ACASA and WRF-NOAH models overestimate the daytime reference ET over these two sites during the spring and summer seasons, the biases in the WRF-ACASA simulations are smaller than the WRF-NOAH simulations. The time series graphs in Fig. 5 and Fig. 6 also show that WRF-ACASA simulations are closer to the observed values. Consequently, the WRF-NOAH model overestimates the annual cumulative ETo compared WRF-ACASA.

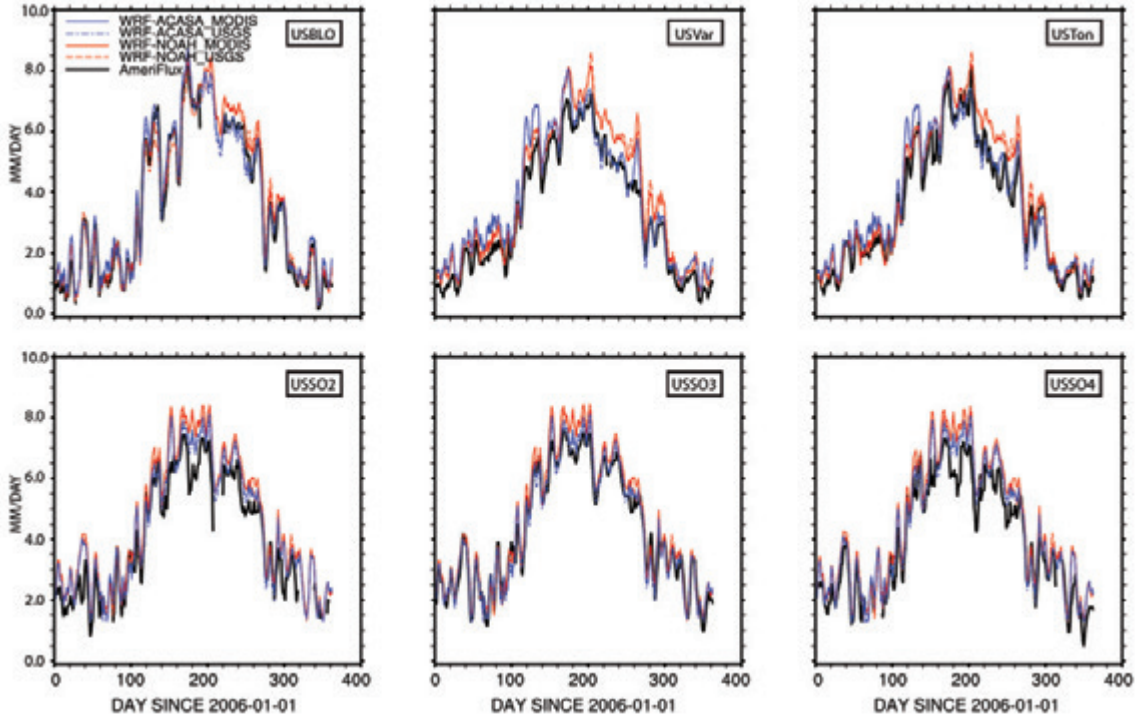


Figure 6. Time series of reference evapotranspiration for the AmeriFlux sites. The solid black line represents observation. The blue lines are for WRF-ACASA, and the red lines are for WRF-NOAH. The solid lines are simulations with MODIS LAI, and the dashed lines are simulations with USGS LAI.

The Taylor diagram in **Fig. 8** illustrates the relative accuracy of the WRF-ACASA and WRF-NOAH models to the observational data for daily ETo, 2 m temperature, dew point temperature, wind speed and solar radiation in each of the four seasons. Using three non-dimensional statistical parameters (the ratio of the variances, the correlation between the two fields, and the RMSE), the Taylor diagram quantifies how well the each model simulates an observed meteorological field with each LAI dataset. Even though the differences in the LAI values shown in Fig. 1 are large, the impact of LAI on surface variables appears small. The largest impact is from model complexity. Generally in all four seasons, the 2 m air temperatures are well simulated by both WRF-ACASA and WRF-NOAH models. However, both models are comparatively poor at simulating wind speed throughout the year. This disparity in wind speed simulation could be due to the difference measurement heights and more general model and station discretization. In the models, wind speeds are simulated at 10-meter height, whereas the observed wind speeds are measured at 2 m height. Therefore, surface measurements of wind speed do not identically match with the standard output from the WRF models. Despite the empirical relationship used to estimate the 2 m wind speed from the simulated 10 m wind speed values, the correlations are still low (Allen *et al.*, 2005).

$$u_2 = u_z \left(\frac{4.87}{\ln(67.8 \cdot z - 5.42)} \right) \quad (5)$$

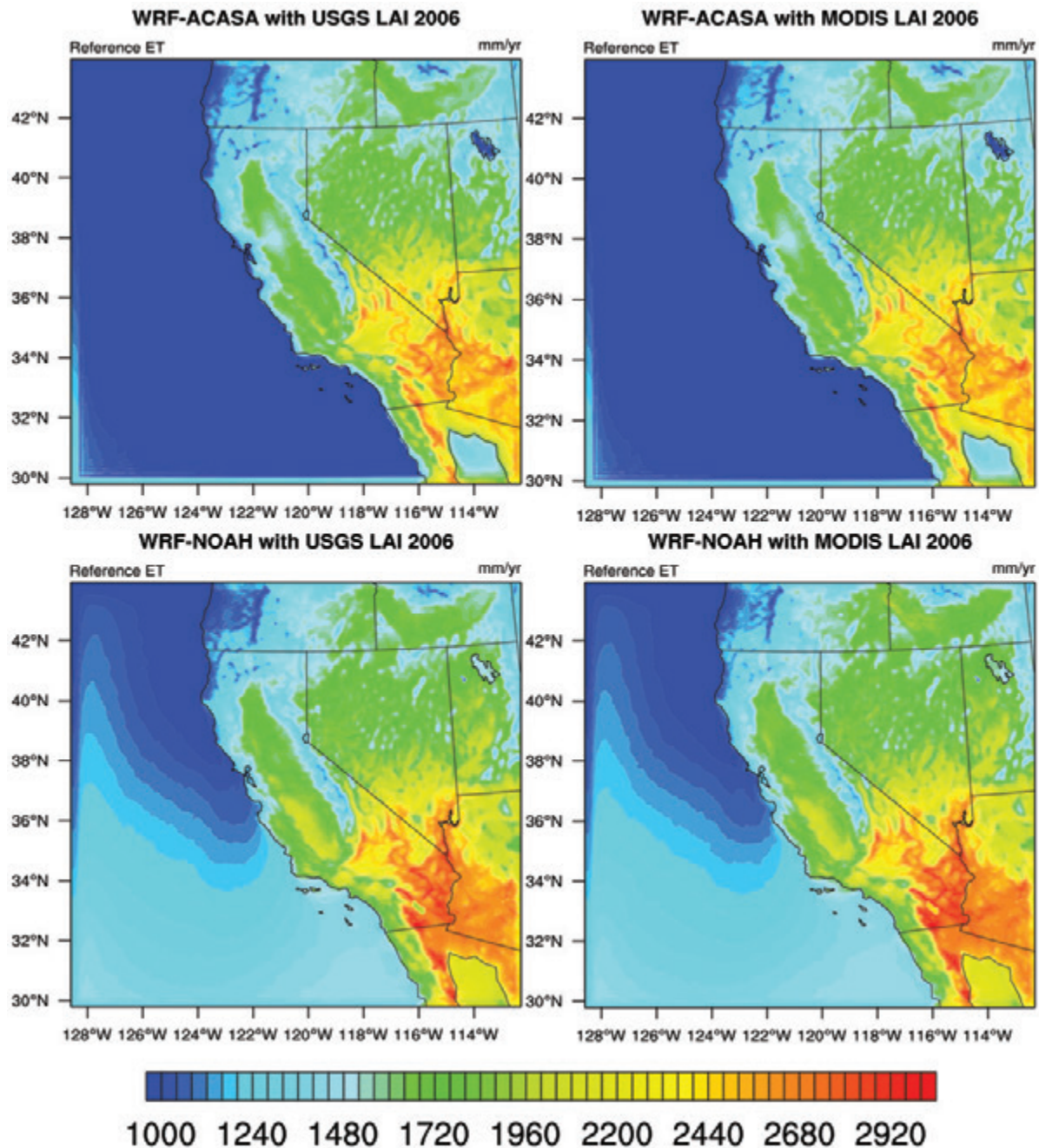


Figure 7. Maps of ETo simulated by WRF-ACASA and WRF-NOAH using USGS (Left panels) and MODIS LAI (Right panels) for 2006. The top panels are WRF-ACASA simulations and the bottom panels are WRF-NOAH simulations.

During the winter, the ETo simulations from both models have reasonable correlations with the surface observations but the RMSEs are high with a large amount of variability in the standard deviations. This could be due to the bias from the wind speed and dew point temperature simulations used in the Penman-Monteith equation to calculate ETo. The reduction in both dew point temperature variability and RMSE of wind speed during the spring seems to improve ETo simulations. The sudden reduction across all statistical variables in the ETo simulations seems to be caused by the poor performance of net downward shortwave radiation.

Taylor Diagram: Model vs. CIMIS 2006

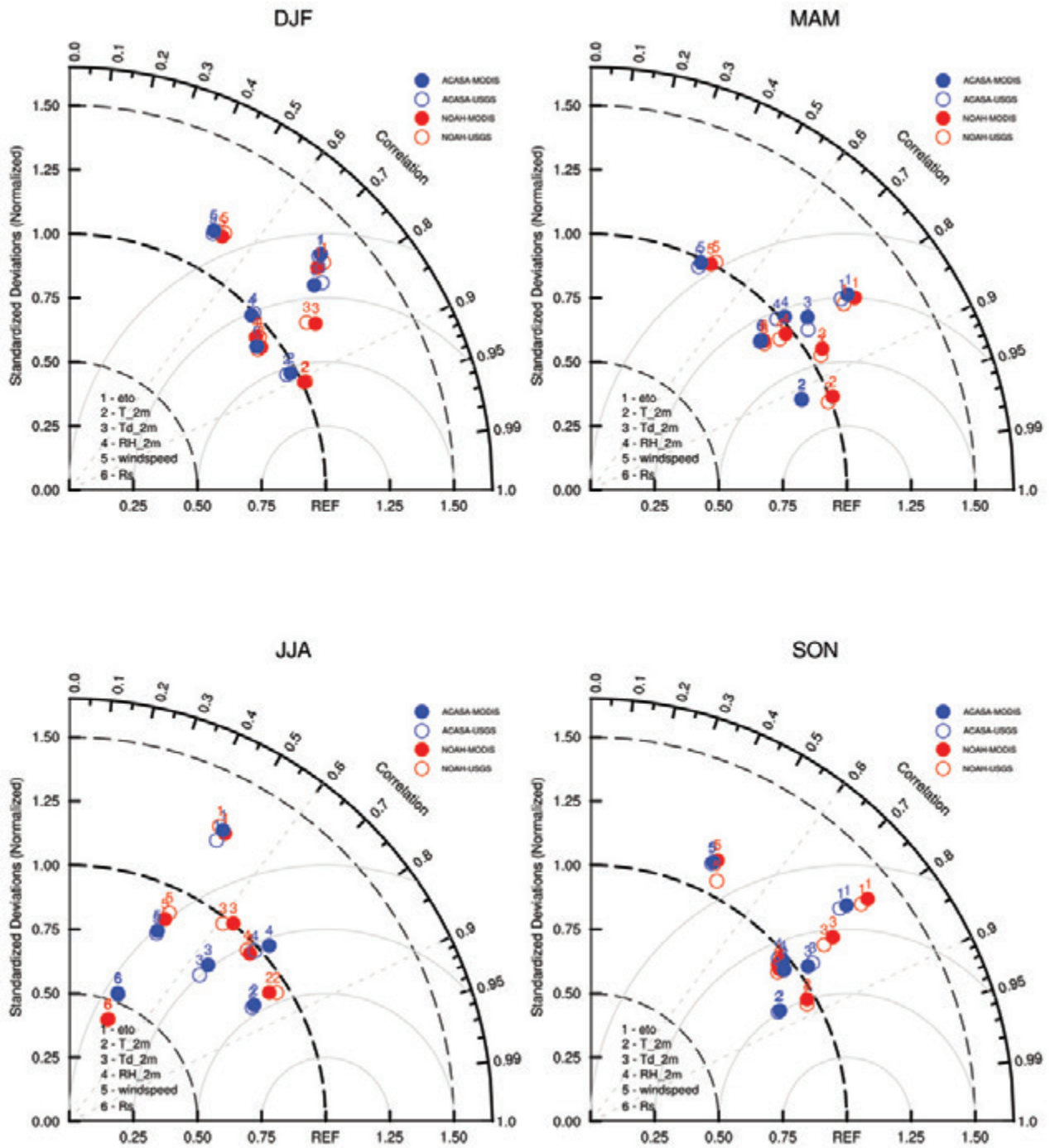


Figure 8. Seasonal Taylor Diagram for the four WRF simulations vs. CIMIS station measurements for daily ETo, 2 m temperature (T_{2m}), dew point temperature (Td_{2m}), wind speed (windspeed), and solar radiation (Rs). Blue represents WRF-ACASA simulations, red represents WRF-NOAH, open circles are simulations using USGS LAI, and solid dots are simulations using MODIS LAI. Winter is DJF, spring is MAM, summer is JJA, and autumn is SON.

3.2 Actual Evapotranspiration

Fig. 9 shows the seasonal diurnal patterns of ET_a of the four WRF simulations and WRF-ACASA with PFT correction for the six AmeriFlux stations. While the differences in model complexity and leaf area index data do not have major influence on ET_o, the ET_a graphs show otherwise. The measured leaf area index in the MODIS LAI dataset systematically lowers the simulated actual evapotranspiration for all four AmeriFlux stations throughout the seasons. Compared to WRF-NOAH model, WRF-ACASA is more influenced by the choice of LAI because it relies on LAI in multiple ways: in the radiation transfer equations, as a direct multiplier of the physiologically determined latent energy flux density per leaf class, and as multipliers to the leaf drag elements affecting the simulated turbulence. The NOAH model uses the LAI only to reduce the canopy resistance through an inverse relationship.

Fig. 10 shows the time series of daily cumulative ET_a from all five WRF model runs and the AmeriFlux measurements. Similar effects of LAI on the diurnal pattern of ET_a in Fig. 9 are also seen in the time series of Fig. 10. The time series again show the impacts of the model complexity and canopy structure on the actual evapotranspiration simulations. Over the Blodgett forest, where PFTs from the model and surface observation match well, the more complex WRF-ACASA model generally outperforms the WRF-NOAH model. The tall and dense canopy of the Blodgett forest is ideal for using the multilayer structure of the WRF-ACASA model. The complex canopy representation and their plant physiological processes more accurately describe the light penetration and inter-canopy mixing, resulting in a better ET_a simulation. The same does not seem to apply to the Tonzi Ranch due to underestimation of canopy openness when the WRF-ACASA model assumes horizontal homogeneity of closed forest in each grid cell. At the same time and over the same grid cell as the Tonzi Ranch, both models overestimated the ET_a during the summer for the Vaira Ranch site, where the grassland growing season is confined only to the wet season from October to early May. The differences in surface conditions and vegetation types of the Vaira Ranch and Tonzi Ranch sites resulted in very different ET_a values even though they are close to each other, thus sharing the same model grid cell.

Overall, increased accuracy of LAI representation from climatological USGS LAI to the remote-sensed MODIS LAI improves the ET_a calculation in both WRF-ACASA and WRF-NOAH models. This improved LAI helped to reduce the RMSE of model simulation by an average of 0.516 mm/day (**Table 2**). This improvement is larger on the WRF-ACASA model than the WRF-NOAH model because of the manner in which LAI impacts multiple processes and layers in ACASA compared to the single layer and simplified processes of NOAH.

Table 2. ET_a RMSE from LAI datasets. Improvement = RMSE (MODIS) - RMSE(USGS).

RMSE	Average	WRF-ACASA	WRF-NOAH
USGS	1.3907	1.9225	0.8590
MODIS	0.8746	1.0431	0.7061
Improvement	-0.5161	-0.8793	-0.1529

In addition to LAI, PFT plays an important role in the high-complexity WRF-ACASA model. At the Sky Oaks sites, the combination of the PFT mismatch and higher LAI in the USGS LAI

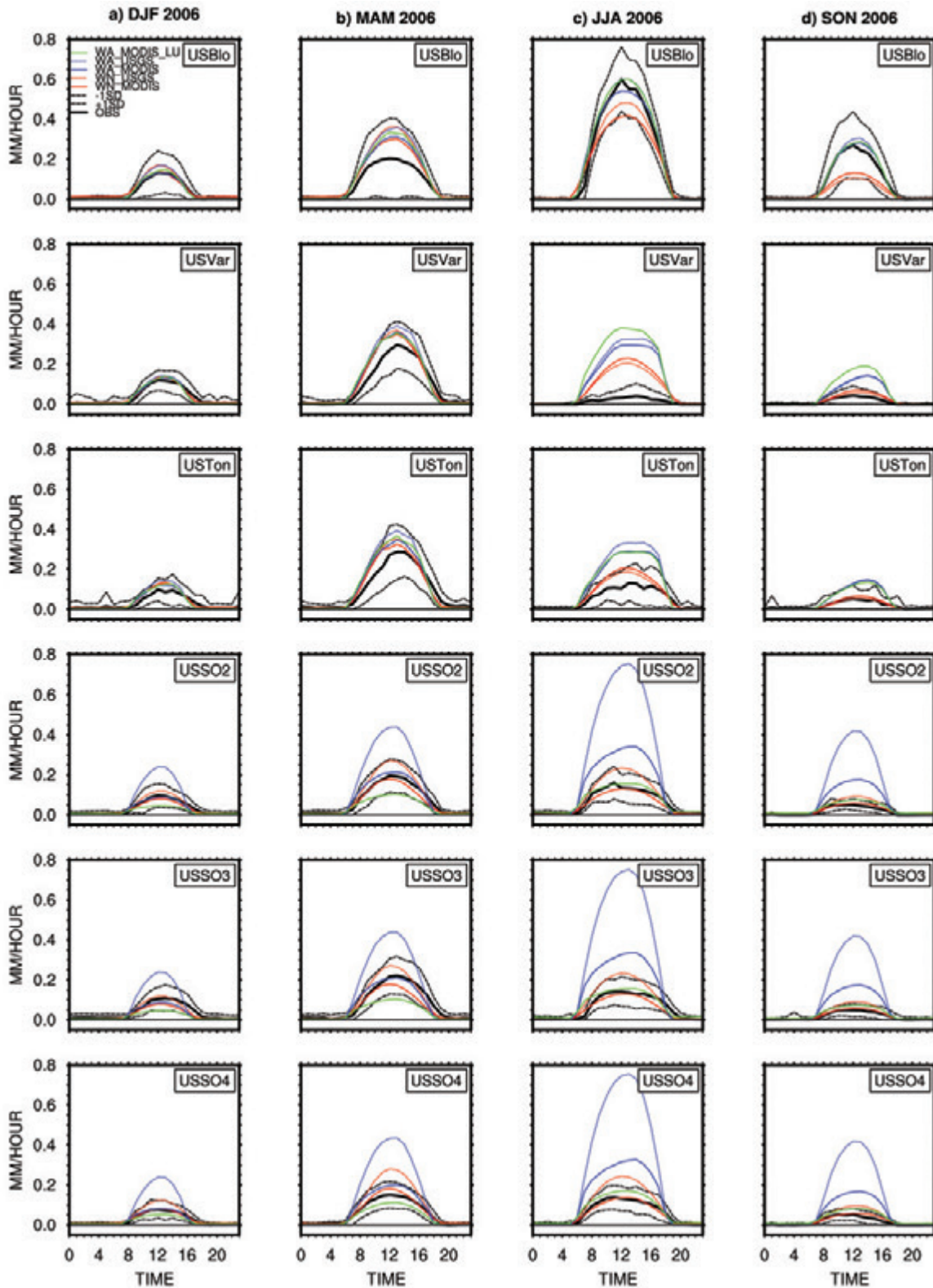


Figure 9. Diurnal patterns of the actual ET for 2006. Red, blue, and green lines are WRF-NOAH, WRF-ACASA, and WRF-ACASA with PFT correction, black is observation. Color dash and solid lines are for USGS and MODIS respectively. Dash black lines are for $\pm 1SD$ of observation.

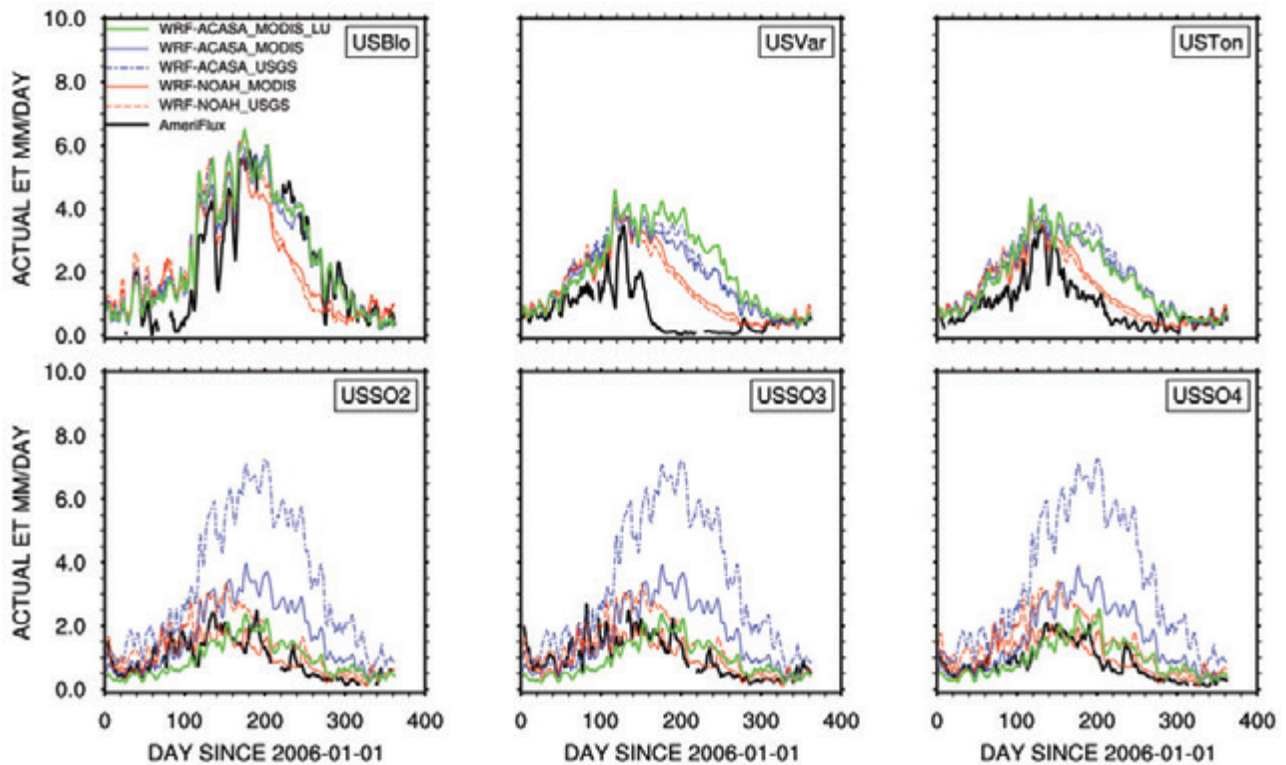


Figure 10. The time series of cumulative daily ETa for the six AmeriFlux sites during 2006. The black lines are surface measurement of daily ETa, the blue lines are WRF-ACASA simulations, and the red lines are WRF-NOAH simulations. The model simulations with MODIS LAI are presented using solid lines and the dash lines are WRF models with USGS LAI.

dataset drive WRF-ACASA to overestimate ETa. Although the more accurate MODIS LAI greatly reduce the bias, the PFT still has a considerable effect, especially over summer and fall seasons. In effort to correct the PFT bias, the PFT of the WRF grid cell, where the Sky Oak sites are located, is reassigned from Evergreen Needleleaf Forest to shrubland to match the Sky Oak 3 and Sky Oak 4 sites. The green lines in both Fig. 9 shows the updated WRF-ACASA ETa Diurnal Cycle for the two sites using MODIS LAI; while Fig. 10 shows the updated ETa time series. Improvement in both PFT and LAI greatly increase the agreement between the WRF-ACASA simulations and observations. These emphasize the importance of surface representations such as land cover type and leaf area index in model simulations. The impact of PFT reassignment for the Sky Oak site on WRF-NOAH is negligible compared to the impact on WRF-ACASA, thus it is not shown.

The simulated annual cumulative ETa data are shown in **Fig. 11**. There are large differences between the WRF-ACASA with MODIS LAI and USGS LAI, but these differences are not visible in the WRF-NOAH simulations. The most significant differences in ETa occur over the Central Valley, and northern California, which align closely with the differences in LAI shown in Fig. 1. This is expected, since LAI is included in several processes in the WRF-ACASA model. In contrast, the WRF-NOAH model only uses LAI in the scaling of the canopy resistance. An overestimation of LAI will cause WRF-ACASA to overestimate ETa. The stomatal closure issues

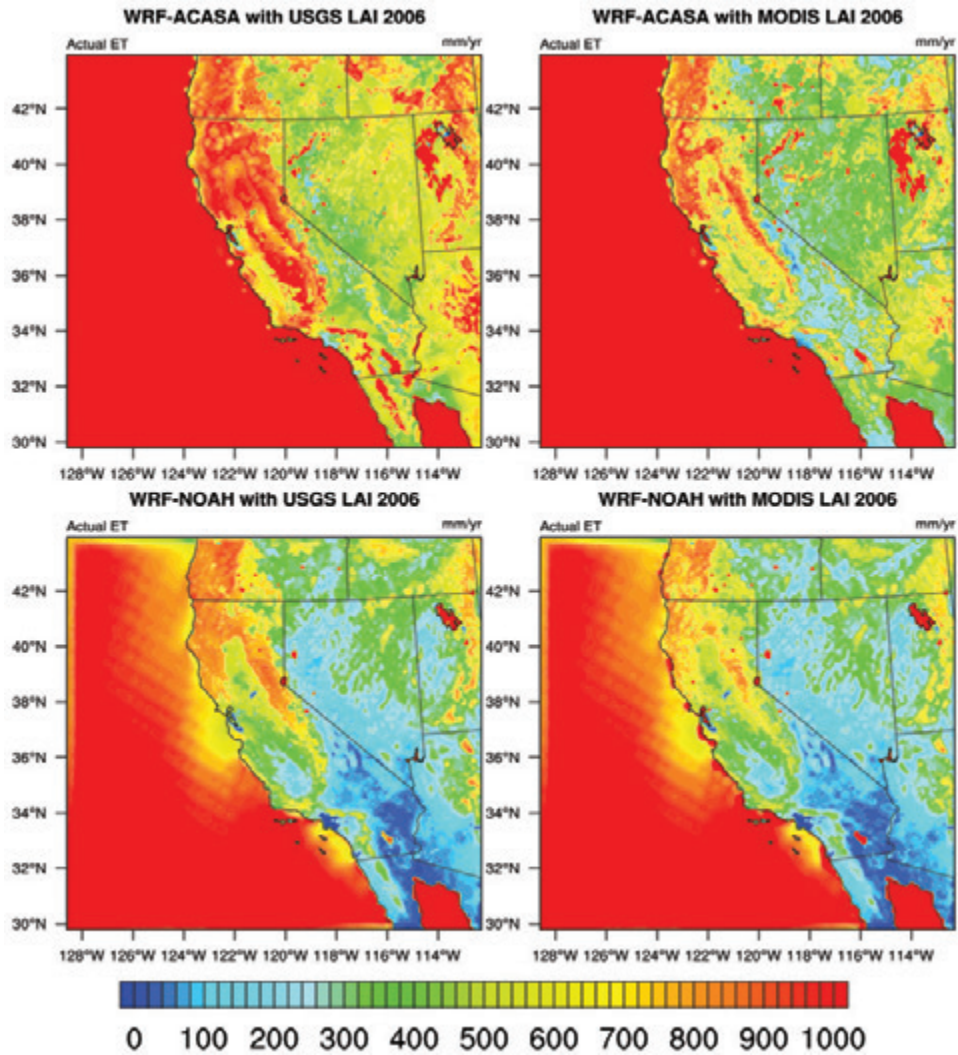


Figure 11. Maps of ET_a simulated by WRF-ACASA and WRF-NOAH using USGS (Left panels) and MODIS LAI (Right panels) for 2006. The top panels are WRF-ACASA simulations and the bottom panels are WRF-NOAH simulations.

shown in the previous graphs are also persistent in the annual timescale, where ET_a values over the southern regions are overestimated compared to corresponding values from the WRF-NOAH simulations. Thresholds in soil moisture for stomatal closure might be set too high, resulting in unrealistic stomatal opening over warm and dry regions of the Mojave Desert. The difference between MODIS LAI and USGS LAI in WRF-NOAH is small, as noted earlier; this may be related to the fact that NOAH uses LAI only to modify the canopy resistance term, rather than to change any other processes.

The Taylor diagram in **Fig. 12** summarizes the actual evapotranspiration performances of the five simulations over the six AmeriFlux sites using WRF-ACASA with USGS, WRF-ACASA with MODIS, and WRF-ACASA with MODIS and PFT bias correction, WRF-NOAH with USGS, and WRF-NOAH with MODIS. The figure shows that the impacts of LAI on land surface models depend on the complexity of the model. While the effect of LAI is to improve ET_a simulations

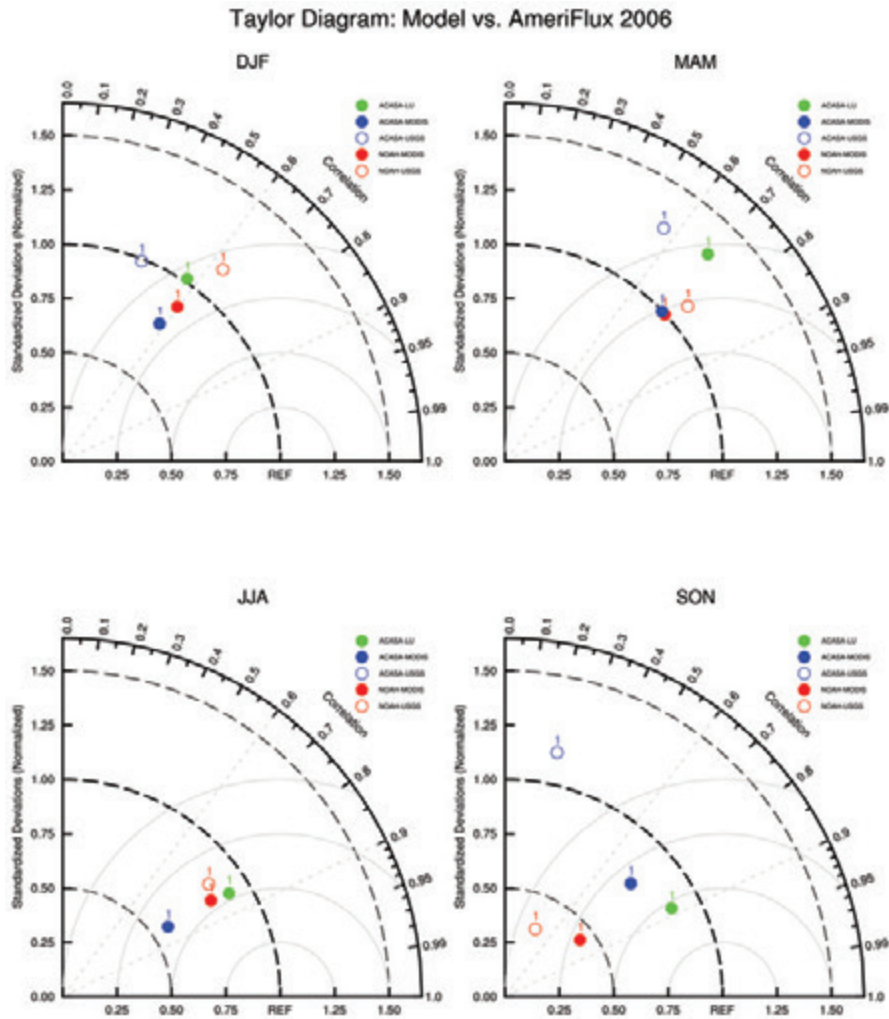


Figure 12. Seasonal Taylor diagram for model simulations and surface measurements of ETa over six AmeriFlux sites for 2006. Blue circle is WRF-ACASA with USGS LAI, blue solid dot is WRF-ACASA with MODIS LAI; red circle is WRF-NOAH with USGS LAI, red solid dot is WRF-NOAH with MODIS LAI; green solid dot is WRF-ACASA with MODIS LAI and PFT bias correction. Winter is DJF (December, January, February), spring is MAM (March, April, May), summer is JJA (June, July, August), and fall is SON (September, October, November).

in both WRF-ACASA and WRF-NOAH, the high complexity WRF-ACASA model benefits the most from the increase in leaf area index accuracy. For example, WRF-ACASA simulations using USGS LAI show poor correlations with surface observation during summer (June, July, and August) and fall (September, October, and November); however, when MODIS LAI is used to improve the surface representation, the ETa simulations also improved. The medium complexity WRF-NOAH model shows much smaller improvements of ETa when using MODIS LAI than the WRF-ACASA model. Furthermore, correcting the grid cell PFT in WRF over Sky Oak 3 and Sky Oak 4 sites to match the observed PFTs, ETa simulations from WRF-ACASA with MODIS LAI vastly improve during summer (JJA) and fall (SON) seasons when compared with surface observation.

The sensitivities of LAI and PFT in WRF simulations using ACASA versus NOAH are due to

the differences in surface representation between the WRF-ACASA and WRF-NOAH models. Unlike the single layer “big leaf” model of the WRF-NOAH, each of the plant functional types in the WRF-ACASA model is associated with a different multilayer canopy structure. While the representation of each PFT with specific canopy structures and plant physiological process allows a more realistic surface representation, these complex relationships are more dependent on the quality of input variables such as land cover type and leaf area index. For example, the model PFT identifies Sky Oaks sites as physiologically active (throughout the year) evergreen needle leaf forest, when in reality they are low-LAI, seasonally inactive, vegetated savanna and scrublands. This affects physiological processes in WRF-ACASA, causing overestimation of ET_a; however, the single-layer WRF-NOAH relies less on the land cover representation and is therefore less sensitive to changes in land surface type designation. Improvements in surface representation of LAI and PFT help increase the accuracy of the high complexity WRF-ACASA model more than the medium complexity WRF-NOAH model.

4. SUMMARY AND CONCLUSION

In this study, the mesoscale model WRF is used to simulate ET_o and ET_a for locations with different combinations of two land surface models and two LAI datasets to examine the impacts that surface representations and model complexity have on ET_o and ET_a. The two land surface models are the intermediate complexity NOAH land surface model and high complexity ACASA model. The two LAI datasets used in the models are from the USGS and MODIS. There are four model simulations: WRF-ACASA with USGS LAI, WRF-ACASA with MODIS LAI, WRF-NOAH with USGS LAI, and WRF-NOAH with MODIS LAI, plus an addition ET_a simulation using WRF-ACASA with MODIS LAI and PFT bias correction. Each simulation was run for the years 2005 and 2006 over all of California and adjacent terrain, but only results from 2006 are shown.

The model results were evaluated using surface observations from the 120 CIMIS network stations for ET_o and from the six AmeriFlux stations for both ET_o and ET_a. Sensitivity tests were employed to evaluate the impacts of differences in surface representations (in both LAI and PFT) and model complexity on simulated ET_o and ET_a in diverse environmental conditions. The results from these four simulations show that an increase in leaf area index accuracy generally improves estimates of ET_a for both the WRF-ACASA and WRF-NOAH models, but it has little effect on ET_o. In addition to LAI, the land use cover or PFT also impacts on simulations of ET_a. When PFTs are bias corrected to match surface observation and model assumption, the more complex WRF-ACASA had great accuracy in its ET_a simulations. In the high complexity WRF-ACASA model, the plant functional type determines the multilayer canopy structure as well as plant physiological parameters. As a result, it is more sensitive to the land cover type than the single-layer WRF-NOAH model.

In conclusion, surface representations such as LAI and PFT appear to impact the detailed plant physiological processes calculations such as ET_a. How the overall representation affects surface processes, however, depends on the model complexity. As the model complexity increases, the model sensitivity to surface representation also increases. The surface processes of

the WRF-ACASA model are more sensitive to the leaf area index than the simple, single layer WRF-NOAH model. The WRF-ACASA model is also sensitive to land use cover, whereas the WRF-NOAH model is not. The two Taylor diagrams for CIMIS stations and AmeriFlux stations do not show significant improvement in ETo or other meteorological variables with improved LAI. There is, however, a small improvement of ETo in the WRF-ACASA when MODIS LAI is used instead of the USGS LAI.

While the high complexity of WRF-ACASA increases the realism of the plant physiological processes, it must be coupled with high accuracy in land surface representation in both leaf area index and land use cover. Consequently, there is a linear relationship between the model complexity and data quality in surface representation. The lower complexity land surface model is less restricted, thus providing more flexibility when high accuracy data is not available. Higher complexity models, however, perform better over more diverse ecosystems such as forests. Depending on the target variables and study areas of interest, the model complexity and surface representation requirements vary.

Further improvement in simulating surface processes such as evapotranspiration can be achieved by improving the model grid cell representation. Both WRF-ACASA and WRF-NOAH models assume one dominant plant functional type in each grid cell. The AmeriFlux data, then again, show that such homogeneous representation of PFT is inaccurate. For example, the Vaira Ranch and the Tonzi Ranch share the same grid cell while the actual surface and environmental conditions of the two sites are different. This error in grid cell representation is also true for the three Sky Oak sites. Instead of using only one dominant PFT in each grid cell, future simulations of land surface processes can be improved by using a combination of PFTs in each grid cell. Although the impact of heterogeneous land use cover in each grid cell may not greatly affect low- or even moderate-complexity models such as WRF-NOAH, it could benefit high-complexity models such as the WRF-ACASA model.

Acknowledgements

This work is supported in part by the National Science Foundation under Awards No.ATM-0619139 and EF-1137306. The Joint Program on the Science and Policy of Global Change is funded by a number of federal agencies and a consortium of 40 industrial and foundation sponsors. (For the complete list see <http://globalchange.mit.edu/sponsors/current.html>).

5. REFERENCES

- Abramowitz, G., R. Leuning, M. Clark and A. Pitman, 2008: Evaluating the performance of land surface models. *J. Climate*, **21**(21): 5468–5481.
- Allen, R., I. Walter, R. Elliott, T. Howell, D. Itenfisu, M. Jensen and R. Snyder, 2005: *The ASCE standardized reference evapotranspiration equation*. American Society of Civil Engineers.
- Bounoua, L., G. Collatz, S. Los, P. Sellers, D. Dazlich, C. Tucker and D. Randall, 2000: Sensitivity of climate to changes in NDVI. *J. Climate*, **13**(13): 2277–2292.
- Chase, T., R. Pielke, T. Kittel, R. Nemani and S. Running, 1996: Sensitivity of a general circulation model to global changes in leaf area index. *J. Geophys. Res.*, **101**: 7393–7408.

- Chen, F. and J. Dudhia, 2001a: Coupling an advanced land surface-hydrology model with the Penn State-NCAR MM5 modeling system. Part I: Model implementation and sensitivity. *Mon. Wea. Rev.*, **129**(4): 569–585.
- Chen, F. and J. Dudhia, 2001b: Coupling an advanced land surface-hydrology model with the Penn State-NCAR MM5 modeling system. Part II: Preliminary model validation. *Mon. Wea. Rev.*, **129**(4): 587–604.
- Chen, F., Z. Janjic and K. Mitchell, 1997: Impact of atmospheric surface-layer parameterizations in the new land-surface scheme of the NCEP mesoscale Eta model. *Bound.Lay. Meteorol.*, **85**(3): 391–421.
- Chen, S. and J. Dudhia, 2000: Annual report: WRF physics. *Air Force Weather Agency*.
- Chen, S. and W. Sun, 2002: A one-dimensional time dependent cloud model. *J. Meteor. Soc. Japan*, **80**(1): 99–118.
- Collatz, G., J. Ball, C. Grivet and J. Berry, 1991: Physiological and environmental regulation of stomatal conductance, photosynthesis and transpiration: a model that includes a laminar boundary layer. *Agric. For. Meteorol.*, **54**(2): 107–136.
- Dickinson, R. and A. Henderson-Sellers, 2006: Modelling tropical deforestation: A study of GCM land-surface parametrizations. *Quart. J. Roy. Meteor. Soc.*, **114**(480): 439–462.
- Dirmeyer, P., D. Niyogi, N. de Noblet-Ducoudre, R. Dickinson and P. Snyder, 2010: Impacts of land use change on climate. *Int. J. Climatol.*, **30**(13): 1905–1907.
- Dudhia, J., 1989: Numerical study of convection observed during the winter monsoon experiment using a mesoscale two-dimensional model. *J. Atmos. Sci.*, **46**(20): 3077–3107.
- Farquhar, G., S. Von Caemmerer *et al.*, 1982: Modelling of photosynthetic response to environmental conditions. *Encyclopedia of plant physiology*, **12**: 549–587.
- Gao, X., P. Dirmeyer, Z. Guo and M. Zhao, 2008: Sensitivity of land surface simulations to the treatment of vegetation properties and the implications for seasonal climate prediction. *J. Hydrol.*, **9**(3): 348–366.
- Gutman, G. and A. Ignatov, 1998: The derivation of the green vegetation fraction from NOAA/AVHRR data for use in numerical weather prediction models. *Int. J. Climatol.*, **19**(8): 1533–1543.
- Hales, K., J. Neelin and N. Zeng, 2004: Sensitivity of Tropical Land Climate to Leaf Area Index: Role of Surface Conductance versus Albedo. *J. Climate*, **17**(7): 1459–1473.
- Henderson-Sellers, A., K. McGuffie and A. Pitman, 1996: The project for intercomparison of land-surface parametrization schemes (PILPS): 1992 to 1995. *Clim. Dyn.*, **12**(12): 849–859.
- Houborg, R. and H. Soegaard, 2004: Regional simulation of ecosystem CO₂ and water vapor exchange for agricultural land using NOAA AVHRR and Terra MODIS satellite data. Application to Zealand, Denmark. *Remote Sens. Environ.*, **93**(1): 150–167.

- Jacquemin, B. and J. Noilhan, 1990: Sensitivity study and validation of a land surface parameterization using the HAPEX-MOBILHY data set. *Bound.Lay. Meteorol.*, **52**(1): 93–134.
- Jones, H., 1992: *Plants and microclimate: a quantitative approach to environmental plant physiology*. Cambridge University Press.
- Knyazikhin, Y., J. Glassy, J. Privette, Y. Tian, A. Lotsch, Y. Zhang, Y. Wang, J. Morisette, P. Votava, R. Myneni *et al.*, 1999: MODIS leaf area index (LAI) and fraction of photosynthetically active radiation absorbed by vegetation (FPAR) product (MOD15) algorithm theoretical basis document. NASA Goddard Space Flight Center .
- Leuning, R., 1990: Modelling stomatal behaviour and and photosynthesis of eucalyptus grandis. *Aust. J. Plant Physiol.*, **17**(2): 159–175.
- Levitt, J. *et al.*, 1980: *Responses of plants to environmental stresses. Volume II. Water, radiation, salt, and other stresses*. Ed. 2. Academic Press.
- Mahrt, L. and M. Ek, 1984: The influence of atmospheric stability on potential evaporation. *Collections*.
- Mesinger, F., G. DiMego, E. Kalnay, K. Mitchell, P. Shafran, W. Ebisuzaki, D. Jovic, J. Woollen, E. Rogers, E. Berbery *et al.*, 2006: North American regional reanalysis. *Bull. Amer. Meteor. Soc.*, **87**(3): 343–360.
- Meyers, T., 1985: A simulation of the canopy microenvironment using higher order closure principles.
- Meyers, T. and K. Paw U, 1987: Modelling the plant canopy micrometeorology with higher-order closure principles. *Agric. For. Meteor.*, **41**(1): 143–163.
- Mlawer, E., S. Taubman, P. Brown, M. Iacono and S. Clough, 1997: Radiative transfer for inhomogeneous atmospheres: RRTM, a validated correlated-k model for the longwave. *J. Geophys. Res.*, **102**(D14): 16663–16.
- Pitman, A., M. Zhao and C. Desborough, 1999: Investigating the sensitivity of a land surface schemes simulation of soil wetness and evaporation to spatial and temporal leaf area index variability within the Global Soil Wetness Project. *J. Meteor. Soc. Japan*, **77**: 281–290.
- Potter, C., J. Randerson, C. Field, P. Matson, P. Vitousek, H. Mooney and S. Klooster, 1993: Terrestrial ecosystem production: a process model based on global satellite and surface data. *Global Biogeochem. Cycles*, **7**(4): 811–841.
- Pyles, R., 2000: The development and testing of the UCD Advanced Canopy–Atmosphere–Soil Algorithm (ACASA) for use in climate prediction and field studies.
- Pyles, R., B. Weare and K. Paw U, 2000: The UCD Advanced Canopy-Atmosphere-Soil Algorithm: comparisons with observations from different climate and vegetation regimes. *Quart. J. Roy. Meteor. Soc.*, **126**: 2951–2980.

- Shuttleworth, W., 1984: Observations of radiation exchange above and below Amazonian forest. *Quart. J. Roy. Meteor. Soc.*, **110**(466): 1163–1169.
- Su, H., K. Paw U and R. Shaw, 1996: Development of a coupled leaf and canopy model for the simulation of plant-atmosphere interactions. *J. Appl. Meteor.*, **35**: 733–748.
- Xu, L., R. D. Pyles, K. T. Paw U, S. H. Chen and E. Monier, 2014: Coupling the high-complexity land surface model ACASA to the mesoscale model WRF. *Geoscientific Model Development*, **7**(6): 2917–2932. doi:[10.5194/gmd-7-2917-2014](https://doi.org/10.5194/gmd-7-2917-2014), 2014.
- Zhan, X. and W. Kustas, 2001: A coupled model of land surface CO₂ and energy fluxes using remote sensing data. *Agric. For. Meteor.*, **107**(2): 131–152.

REPORT SERIES of the MIT Joint Program on the Science and Policy of Global Change

FOR THE COMPLETE LIST OF JOINT PROGRAM REPORTS: <http://globalchange.mit.edu/pubs/all-reports.php>

249. **Limited Sectoral Trading between the EU ETS and China.** *Gavard et al.*, August 2013
250. **The Association of Large-Scale Climate Variability and Teleconnections on Wind Resource over Europe and its Intermittency.** *Kriesche and Schlosser*, September 2013
251. **Regulatory Control of Vehicle and Power Plant Emissions: How Effective and at What Cost?** *Paltsev et al.*, October 2013
252. **Synergy between Pollution and Carbon Emissions Control: Comparing China and the U.S.** *Nam et al.*, October 2013
253. **An Analogue Approach to Identify Extreme Precipitation Events: Evaluation and Application to CMIP5 Climate Models in the United States.** *Gao et al.* November 2013
254. **The Future of Global Water Stress: An Integrated Assessment.** *Schlosser et al.*, January 2014
255. **The Mercury Game: Evaluating a Negotiation Simulation that Teaches Students about Science–Policy Interactions.** *Stokes and Selin*, January 2014
256. **The Potential Wind Power Resource in Australia: A New Perspective.** *Hallgren et al.*, February 2014
257. **Equity and Emissions Trading in China.** *Zhang et al.*, February 2014
258. **Characterization of the Wind Power Resource in Europe and its Intermittency.** *Cosseron et al.*, March 2014
259. **A Self-Consistent Method to Assess Air Quality Co-Benefits from US Climate Policies.** *Saari et al.*, April 2014
260. **Electricity Generation and Emissions Reduction Decisions under Policy Uncertainty: A General Equilibrium Analysis.** *Morris et al.*, April 2014
261. **An Integrated Assessment of China's Wind Energy Potential.** *Zhang et al.*, April 2014
262. **The China-in-Global Energy Model.** *Qi et al.* May 2014
263. **Markets versus Regulation: The Efficiency and Distributional Impacts of U.S. Climate Policy Proposals.** *Rausch and Karplus*, May 2014
264. **Expectations for a New Climate Agreement.** *Jacoby and Chen*, August 2014
265. **Coupling the High Complexity Land Surface Model ACASA to the Mesoscale Model WRF.** *Xu et al.*, August 2014
266. **The CO₂ Content of Consumption Across US Regions: A Multi-Regional Input-Output (MRIO) Approach.** *Caron et al.*, August 2014
267. **Carbon emissions in China: How far can new efforts bend the curve?** *Zhang et al.*, October 2014
268. **Characterization of the Solar Power Resource in Europe and Assessing Benefits of Co-Location with Wind Power Installations.** *Bozonnat and Schlosser*, October 2014
269. **A Framework for Analysis of the Uncertainty of Socioeconomic Growth and Climate Change on the Risk of Water Stress: a Case Study in Asia.** *Fant et al.*, November 2014
270. **Interprovincial Migration and the Stringency of Energy Policy in China.** *Luo et al.*, November 2014
271. **International Trade in Natural Gas: Golden Age of LNG?** *Du and Paltsev*, November 2014
272. **Advanced Technologies in Energy-Economy Models for Climate Change Assessment.** *Morris et al.*, December 2014
273. **The Contribution of Biomass to Emissions Mitigation under a Global Climate Policy.** *Winchester and Reilly*, January 2015
274. **Modeling regional transportation demand in China and the impacts of a national carbon constraint.** *Kishimoto et al.*, January 2015.
275. **The Impact of Advanced Biofuels on Aviation Emissions and Operations in the U.S.** *Winchester et al.*, February 2015
276. **Specifying Parameters in Computable General Equilibrium Models using Optimal Fingerprint Detection Methods.** *Koesler*, February 2015
277. **Renewables Intermittency: Operational Limits and Implications for Long-Term Energy System Models.** *Delarue and Morris*, March 2015
278. **The MIT EPPA6 Model: Economic Growth, Energy Use, and Food Consumption.** *Chen et al.*, March 2015
279. **Emulating maize yields from global gridded crop models using statistical estimates.** *Blanc and Sultan*, March 2015
280. **Water Body Temperature Model for Assessing Climate Change Impacts on Thermal Cooling.** *Strzepek et al.*, May 2015
281. **Impacts of CO₂ Mandates for New Cars in the European Union.** *Paltsev et al.*, May 2015
282. **Natural Gas Pricing Reform in China: Getting Closer to a Market System?** *Paltsev and Zhang*, July 2015
283. **Global population growth, technology, and Malthusian constraints: A quantitative growth theoretic perspective.** *Lanz et al.*, October 2015
284. **Capturing Natural Resource Dynamics in Top-Down Energy-Economic Equilibrium Models.** *Zhang et al.*, October 2015
285. **US Major Crops' Uncertain Climate Change Risks and Greenhouse Gas Mitigation Benefits.** *Sue Wing et al.*, October 2015
286. **Launching a New Climate Regime.** *Jacoby and Chen*, November 2015
287. **Impact of Canopy Representations on Regional Modeling of Evapotranspiration using the WRF-ACASA Coupled Model.** *Xu et al.*, December 2015